Silicon Photonic Micro-Ring Resonator Biosensors: Principles, Performance, and Biomedical Applications

Kosar Khodami
Dept. of Electronics, Information and Bioengineering
Politecnico di Milano
kosar.khodami@mail.polimi.it

Abstract

Silicon photonic micro-ring resonators (MRRs) have emerged as one of the most promising platforms for label-free biosensing. This review covers their working principles, key performance metrics, and advanced sensitivity-enhancement configurations, including slot waveguides, subwavelength grating structures, and the Vernier effect in cascaded resonator systems. Reported bulk sensitivities range from 112 nm/RIU for a single ring resonator to 21,500 nm/RIU for Vernier-effect cascaded MRR-MZI systems. Biomedical applications in cancer cell and biomarker detection are reviewed alongside remaining fabrication and integration challenges.

I. Introduction

The convergence of silicon photonics and biosensing has produced a new generation of analytical devices capable of detecting molecular interactions in real time, without labels, and at the chip scale. Among the configurations available on silicon-on-insulator (SOI) – Mach–Zehnder interferometers (MZIs), photonic crystal (PhC) cavities, Bragg gratings, and micro-ring resonators – the MRR stands out for its compact footprint, high quality factor, and natural compatibility with dense multiplexed sensor arrays [1], [2]. A comprehensive review of silicon photonic biosensor performance metrics is given by Steglich et al. [6], who catalogue sensitivity and limit-of-detection (LoD) values across all major SOI resonator types.

The sensing mechanism relies on the evanescent field that extends beyond the waveguide core. When a target analyte binds to the functionalized ring surface, the local refractive index (RI) changes, shifting the resonant wavelength – the label-free sensor signal. The SOI platform exploits the high RI contrast between silicon (n_{Si} = 3.48) and silicon dioxide (n_{SiO_2} = 1.44), enabling sub-micron waveguides with strong optical confinement [1]. De Vos et al. [4] demonstrated one of the earliest SOI MRR biosensors, achieving a LoD of 1.6×10^{-6} RIU for protein detection in buffer, establishing SOI MRRs as a viable label-free sensing platform.

From the clinical perspective, early cancer detection is a critical unmet need. Cancer cells exhibit RIs of 1.39–1.402, measurably higher than the RI of normal cells ($\approx$1.35) [2]. A chip-integrated array of 32 MRR sensors has been demonstrated for simultaneous quantification of eight cancer biomarkers from patient serum [3], highlighting the multiplexing advantage of this platform for oncology diagnostics.

This paper reviews the physical foundations of MRR sensing (Section II), sensitivity-enhancement strategies (Section III), biosensor architectures (Section IV), biomedical applications (Section V), and open challenges (Section VI).

II. Operating Principle Of MRR Biosensors

A. Resonance Condition

A micro-ring resonator consists of a circular waveguide loop evanescently coupled to a straight bus waveguide. Resonance occurs when the round-trip optical path length equals an integer multiple of the guided wavelength:

$$\lambda_m = \frac{2\pi\, r\, n_{\text{eff}}}{m}, \tag{1}$$

where r is the ring radius, n_{eff} is the effective mode index, and m is the resonance order [2]. At resonance, a sharp dip appears in the bus waveguide transmission spectrum. Any perturbation of n_{eff} due to analyte binding shifts λ_m and constitutes the sensing signal. De Vos et al. [4] provide a detailed experimental characterization of this resonance shift for streptavidin–biotin binding on functionalized SOI rings.

B. Evanescent Field Interaction

The guided mode extends partially into the cladding as an evanescent wave that decays exponentially with perpendicular distance d from the waveguide surface [1]:

$$E(d) = E_0 \exp\left(-\frac{d}{d_p}\right), \qquad d_p = \frac{\lambda}{4\pi\sqrt{n_{\text{eff}}^2 - n_c^2}}, \tag{2}$$

where d_p is the penetration depth and n_c is the cladding RI. For a $220\,\text{nm} \times 500\,\text{nm}$ SOI waveguide at $\lambda = 1550$ nm, the TM mode places more field power above and below the core than the TE mode, resulting in stronger bulk sensitivity at the cost of higher sidewall-scattering losses [1]. This TE/TM trade-off is a well-documented design choice for SOI biosensors reviewed in depth by Steglich et al. [6].

C. Sensitivity and Quality Factor

Two figures of merit dominate MRR sensor design. The bulk sensitivity S_{bulk} is the resonance wavelength shift per unit RI change:

$$S_{\text{bulk}} = \frac{\Delta\lambda}{\Delta n_{\text{fluid}}}, \tag{3}$$

and the surface sensitivity S_{surf} replaces Δn_{fluid} with the adlayer thickness $\Delta t_{\text{adlayer}}$ to characterize monolayer binding events [1]. The quality factor Q governs the sharpness of the resonance dip and hence the minimum detectable wavelength shift:

$$Q = \frac{\lambda_{\text{res}}}{\Delta\lambda_{\text{FWHM}}}, \tag{4}$$

where $\Delta\lambda_{\text{FWHM}}$ is the full-width at half-maximum [2]. Claes et al. [8] experimentally confirmed that high-Q cascaded SOI rings ($Q \sim 10^4$–10^5) achieve LoDs of 8.3×10^{-8} RIU, an order of magnitude below a single ring. The LoD in terms of minimum detectable surface mass density has also been characterized by Steglich et al. [6] for functionalized SOI rings exposed to bovine serum albumin (BSA).

III. Performance Enhancement Strategies

A. Slot Waveguide Integration

In a standard strip waveguide, only $\sim$20% of the guided light interacts with the analyte; in a slot waveguide, two silicon rails separated by a narrow low-RI gap force $>$70% of the guided power into the slot region, in direct contact with the cladding medium [1]. This significantly increases both S_{bulk} and S_{surf}. Liu et al. [7] demonstrated a Si_3N_4 slot-waveguide MZI biosensor achieving $S_{\text{bulk}} = 1{,}300$ nm/RIU with a LoD of 5.4×10^{-6} RIU, a factor of $\sim$3.5 improvement over the equivalent strip waveguide sensor. The same group showed that combining the slot geometry with grating couplers for efficient fiber-to-chip light injection allows robust packaging for microfluidic integration [7].

B. Subwavelength Grating Waveguide

Subwavelength grating (SWG) waveguides replace the homogeneous silicon core with a periodic array of alternating high-index (Si) and low-index (SiO_2 or air) blocks, with a period Λ well below the Bragg condition. The guided mode sees an effective medium whose RI is set by the duty cycle, bringing more optical power into the low-index sensing medium [1]. SWG ring resonators, SWG Bragg gratings – realized by interleaving two SWG waveguides with different duty cycles – and SWG racetrack resonators with extended coupling regions have all been implemented on SOI, each providing enhanced evanescent field overlap compared to conventional strip waveguides [1].

C. Vernier Effect in Cascaded Configurations

The most powerful enhancement exploits the Vernier effect by cascading two rings (or a ring and an MZI) with slightly different free spectral ranges (FSRs). If the sensing ring has FSR_1 and the reference ring has FSR_2, the envelope of the combined spectrum shifts with a magnification factor:

$$M = \frac{\text{FSR}_1}{|\text{FSR}_1 - \text{FSR}_2|}. \tag{5}$$

Claes et al. [8] experimentally demonstrated cascaded SOI MRRs with FSRs of 10.09 nm and 10.66 nm, yielding $M \approx 17.7$ and a measured $S_{\text{bulk}} = 2{,}169$ nm/RIU – a 19-fold improvement over a single ring. Extending the concept to a cascaded MZI-ring configuration, Jiang et al. [5] reported $S_{\text{bulk}} = 21{,}500$ nm/RIU, with the MZI providing 2,870 nm/RIU as a standalone, giving a 7.5$\times$ Vernier gain. These values, alongside other configurations, are compared in Table I and Fig. 1(b).

TABLE I
PERFORMANCE COMPARISON OF MRR-BASED SENSOR CONFIGURATIONS

Configuration	S_{bulk} *(nm/RIU)*	*LoD (RIU)*	*Ref.*
Single MRR (SOI)	112	1.6×10^{-6}	[4]
MRR with MZI readout	2.5×10^{3}[a]	1×10^{-8}	[1]
Cascaded MRR (Vernier)	2,169	8.3×10^{-8}	[8]
MZI–Ring (Vernier)	21,500	n.r.	[5]
Ring (disk) resonator	193	7.3×10^{-8}	[1]
Si_3N_4 slot MZI	1,300	5.4×10^{-6}	[7]
Si_3N_4 MRR (cancer)	568	n.r.	[10]

[a]In μm/RIU; n.r. = not reported.

IV. MRR BIOSENSOR ARCHITECTURES

A. Single-Ring and Add-Drop Configurations

The single-ring add-drop configuration uses a second bus waveguide to collect resonant power, improving signal-to-noise ratio. De Vos et al. [4] demonstrated SOI add-drop MRRs with $r = 5\,\mu$m and $Q \approx 20{,}000$, obtaining a LoD of 1.6×10^{-6} RIU and detecting interleukin-6 at concentrations down to 5 ng/mL without labeling. Steglich et al. [6] further showed that dual-polarization readout – tracking both TE and TM resonances of the same ring simultaneously – enables discrimination between bulk RI changes and surface adlayer formation, removing a key ambiguity in single-ring measurements.

B. Chip-Integrated Multiplexed Sensor Arrays

The compact footprint of MRRs allows hundreds of addressable sensors on a single chip. Washburn et al. [3] demonstrated a 32-sensor SOI array with two thermal reference rings for simultaneous quantification of eight cancer biomarkers – AFP, ALCAM, CA-15-3, CA-19-9, CA-125, CEA, osteopontin, and PSA – from 1 mL patient serum in under 60 minutes. Wavelength-division multiplexing (WDM) of the individual ring resonances allows single-laser swept readout, with active thermo-optic tuning aligning each ring to its WDM channel.

C. Suspended MRR Geometry

In suspended MRRs, the ring waveguide is released from the buried oxide to allow analyte contact on both top and bottom surfaces. Gaur et al. [9] applied this geometry to label-free detection of Herceptin (trastuzumab) for breast cancer therapy monitoring, demonstrating approximately double the surface sensitivity of a substrate-supported ring of identical dimensions. Microfluidic packaging for such chip-scale platforms was demonstrated by Adamopoulos et al. [12], who developed 3D-printed PDMS transfer-molded cartridges with <150 μm channel spacing, achieving parallel analyte delivery to multiple ring sensors without cross-contamination in a CMOS back-end compatible process.

V. BIOMEDICAL APPLICATIONS: CANCER CELLS AND BIOMARKERS

A. RI Contrast Of Cancer Cells

The basis for MRR cancer sensing is the measurable RI difference between normal and malignant cells. As summarized by Sajan et al. [2], normal cells have RI $\approx$ 1.35 while cancer cell lines range from HeLa (RI = 1.390) to Jurkat (RI = 1.402). This $\Delta n \approx 0.04$ RIU translates to a resonance shift of $\sim$4.5 nm in a single MRR [4] and $\sim$860 nm in a Vernier MZI-ring system [5] – both resolvable above the noise floor of a thermally stabilized platform [8].

B. Cascaded MRR for Gastric Cancer Detection

In the cascaded two-ring configuration illustrated in Fig. 1(a), one ring (Ring A) is hermetically sealed under a protective cladding and acts as a real-time thermal reference, while the second ring (Ring B) is exposed to the analyte through an open sensing window [2]. An FDTD simulation of this geometry shows a resonance shift of 0.38 nm in Ring B when switching from normal-cell buffer (RI = 1.35) to gastric cancer cell medium (RI = 1.39), as seen in the transmission spectra of Fig. 1(b). The two cell types yield distinct dips below and above 1.85 μm, enabling unambiguous discrimination. Nejad et al. [11] further demonstrated a tunable PhC nanocavity nano-biosensor resolving RI differences as small as 10^{-5} RIU between cell lines, achieving 790 nm/RIU sensitivity for cervical cancer cells at 1550 nm.

C. Silicon Nitride Biosensors for Cancer Biomarkers

Kumaar and Sivasubramanian [10] designed a Si_3N_4 rib-slot waveguide MZI (970 nm wide, 400 nm thick) achieving $S_{\text{bulk}} = 568$ nm/RIU and device sensitivity of 2.07 RIU/RIU, operating on cancer cell blood samples as a bulk analyte solution. The slot-waveguide MZI results of Liu et al. [7] complement this work by confirming that Si_3N_4 slot geometries consistently outperform SOI strip waveguides for bulk analyte sensing, while maintaining compatibility with standard grating-coupler chip interfaces.

D. Multiplexed Cancer Biomarker Quantification

Washburn et al. [3] quantified eight cancer biomarkers simultaneously from patient serum using a chip-integrated SOI MRR array with antibody-functionalized surfaces, achieving clinically relevant LoDs for PSA, CEA, and CA-125 in a one-hour workflow without sample preprocessing. The microfluidic packaging solution developed by Adamopoulos et al. [12] directly supports such platforms by enabling automated multi-stream sample delivery to the chip with no cross-talk.

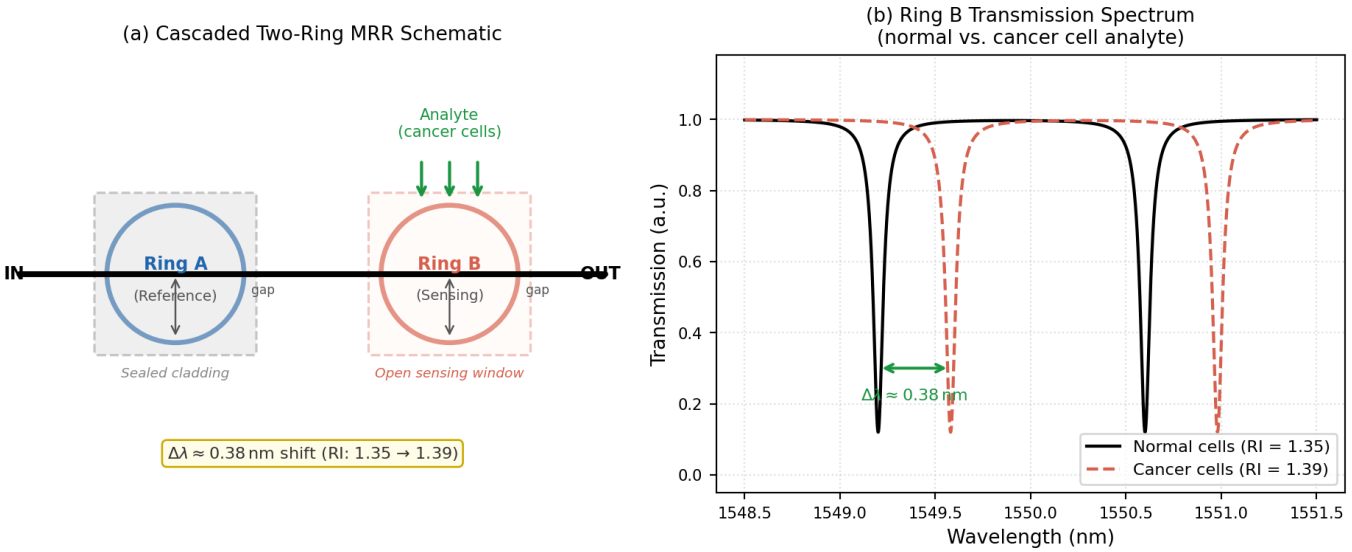

Fig. 1. (a) Schematic of the cascaded two-ring MRR biosensor. Ring A is sealed under a protective cladding and serves as a thermal reference; Ring B has an open sensing window exposed to the analyte. Both rings are evanescently coupled to the same bus waveguide. (b) Simulated transmission spectra of Ring B for normal-cell buffer (RI = 1.35) and gastric cancer cell analyte (RI = 1.39), showing the ≈0.38 nm resonance shift reported in [2]. The shift is the primary sensor signal; thermal drift common to both rings is cancelled by the reference.

VI. Challenges And Future Directions

Despite impressive results, several barriers remain before MRR biosensors achieve routine clinical deployment.

Thermal stability: The silicon thermo-optic coefficient ($dn/dT \approx 1.8 \times 10^{-4}$ K^{-1}) causes resonance drift that can mask weak analyte signals [1]. Claes et al. [8] addressed this using the sealed reference ring of the cascaded system as a real-time drift compensator, reducing temperature-induced noise by an order of magnitude.

Surface biofunctionalization: Selective, high-density antibody immobilization on silicon surfaces is critical for specificity in blood matrices. Steglich et al. [6] review functionalization protocols for SOI MRRs, noting that amine-reactive cross-linking on thermal oxide surfaces offers the best coverage uniformity, while direct silanization of silicon sidewalls remains less reproducible.

On-chip light sourcing: Most platforms couple external tunable lasers via grating couplers, introducing insertion losses of 3–10 dB per facet [2]. Monolithic III-V-on-SOI laser integration is advancing, but foundry-compatible on-chip sources are not yet available at low cost.

Microfluidic packaging: Adamopoulos et al. [12] showed that 3D-printed PDMS cartridges can deliver multiple analyte streams to an SOI chip with no inter-channel cross-talk, but scaling this to wafer-level assembly remains an engineering challenge.

Looking ahead, suspended MRR geometries [9] and the SiON waveguide platform – whose RI is tunable between 1.44 and 2.00 by nitrogen content [2] – offer new design degrees of freedom. The slot-waveguide results of Liu et al. [7] also point toward environmental monitoring as a near-term application, where the sub-ppm sensitivity of Si_3N_4 slot MZIs is well matched to water quality sensing.

VII. Conclusion

Silicon photonic micro-ring resonators have matured into a well-characterized, chip-scale biosensing platform with demonstrated clinical relevance. The resonance condition $\lambda_m = 2\pi r\, n_{\text{eff}}/m$ provides a robust transduction mechanism whose sensitivity can be systematically enhanced – from 112 nm/RIU for a single SOI ring [4] to 21,500 nm/RIU for a Vernier-effect MZI-ring cascade [5] – through slot waveguide geometries [7], SWG structures, and FSR-engineering of cascaded resonators [8]. Multiplexed arrays of 32 rings have simultaneously quantified eight cancer biomarkers from patient serum [3], and suspended MRR geometries [9] extend sensitivity by exposing both ring surfaces to the analyte. The main remaining barriers – microfluidic packaging [12], on-chip light sourcing, and surface chemistry [6] – are all areas of active worldwide research, and their resolution will accelerate the translation of MRR biosensors into point-of-care clinical instruments.

References

[1] C. Dhote, A. Singh, and S. Kumar, "Silicon photonics sensors for biophotonic applications—A review," *IEEE Sensors J.*, vol. 22, no. 19, pp. 18228–18239, Oct. 2022.

[2] S. Cheeran Sajan, A. Singh, P. K. Sharma, and S. Kumar, "Silicon photonics biosensors for cancer cells detection—A review," *IEEE Sensors J.*, vol. 23, no. 4, pp. 3366–3377, Feb. 2023.

[3] A. L. Washburn, W. W. Shia, K. A. Lenkeit, S.-H. Lee, and R. C. Bailey, "Multiplexed cancer biomarker detection using chip-integrated silicon photonic sensor arrays," *Analyst*, vol. 141, no. 18, pp. 5358–5365, 2016.

[4] K. De Vos, I. Bartolozzi, E. Schacht, P. Bienstman, and R. Baets, "Silicon-on-insulator microring resonator for sensitive and label-free biosensing," *Opt. Express*, vol. 15, no. 12, pp. 7610–7615, 2007.

[5] X. Jiang, Y. Chen, F. Yu, L. Tang, M. Li, and J.-J. He, "High-sensitivity optical biosensor based on cascaded Mach-Zehnder interferometer and ring resonator using Vernier effect," *Opt. Lett.*, vol. 39, no. 22, pp. 6363–6366, 2014.

[6] P. Steglich, M. Hulsemann, B. Dietzel, and A. Mai, "Optical biosensors based on silicon-on-insulator ring resonators: A review," *Molecules*, vol. 24, no. 3, p. 519, 2019.

[7] Q. Liu, X. Tu, K. W. Kim, J. S. Kee, Y. Shin, K. Han, Y.-J. Yoon, G.-Q. Lo, and M. K. Park, "Highly sensitive Mach-Zehnder interferometer biosensor based on silicon nitride slot waveguide," *Sens. Actuators B, Chem.*, vol. 188, pp. 681–688, Nov. 2013.

[8] T. Claes, W. Bogaerts, and P. Bienstman, "Experimental characterization of a silicon photonic biosensor consisting of two cascaded ring resonators based on the Vernier-effect," *Opt. Express*, vol. 18, no. 22, pp. 22747–22761, Oct. 2010.

[9] G. Gaur, S. Hu, R. L. Mernaugh, I. I. Kravchenko, S. T. Retterer, and S. M. Weiss, "Label-free detection of Herceptin using suspended silicon microring resonators," *Sens. Actuators B, Chem.*, vol. 275, pp. 394–401, Dec. 2018.

[10] P. Kumaar and A. Sivasubramanian, "Design and bulk sensitivity analysis of a silicon nitride photonic biosensor for cancer cell detection," *Int. J. Opt.*, vol. 2022, pp. 1–9, May 2022.

[11] H. E. Nejad, A. Mir, and A. Farmani, "Supersensitive and tunable nano-biosensor for cancer detection," *IEEE Sensors J.*, vol. 19, no. 13, pp. 4874–4881, Jul. 2019.

[12] C. Adamopoulos, A. Gharia, A. Niknejad, V. Stojanovic, and M. Anwar, "Microfluidic packaging integration with electronic-photonic biosensors using 3D printed transfer molding," *Biosensors*, vol. 10, no. 11, p. 177, Nov. 2020.